Polymer Chemistry

ROYAL SOCIETY OF CHEMISTRY

PAPER

Incorporating polar oxazolidinones into polycyclooctadiene *via* frontal ring-opening metathesis polymerization

Jazmin E. Aguilar-Romero, [ID] † Elizabeth G. Rogan, [ID] † Allison R. Wong, [ID] Brandon M. Hosford, [ID] Angela L. Mosconi and Jessica R. Lamb [ID] *

Frontal ring-opening metathesis polymerization (FROMP) is a rapid, facile method that requires little energy input by utilizing the polymerization exotherm to self-propagate. Although FROMP is efficient, its scope has been limited to highly strained monomers to provide enough energy to drive the polymerization front. Copolymerization has been a viable strategy to introduce more diverse monomers to make polar-functionalized dicyclopentadiene-based thermosets. In contrast, analagous FROMP copolymerizations to produce soluble thermoplastics containing polar repeat units have yet to be explored. Herein, we report the frontal copolymerization of cyclooctadiene (COD) with 1–5 mol% of a lower ring-strain oxazolidinone-fused cyclooctene (Oxa) to synthesize polybutadiene-based copolymers. As expected, as the Oxa loading increased, the front velocity decreased by up to 50% and maximum front temperature decreased by ~16 °C compared to pCOD homopolymer. While the degradation and glass transition temperatures were minimally affected, the polar Oxa units greatly influenced crystallization and tensile properties of the resulting materials. In particular, the ductility dramatically increased from 220% strain at break for pCOD to 1900% for copolymers with 5 mol% Oxa. This study provides an easy method to incorporate polar functionality into ubiquitous polyolefins and further demonstrates the impact of dipoles on material properties towards future applications.

Introduction

Frontal polymerization (FP) is a self-propagating technique that rapidly produces polymers upon initiation by a localized stimulus (Fig. 1A).[1] By only requiring energy input at the start of the reaction and then relying on the polymerization exotherm to propagate the front, FP accesses materials in an energy-efficient manner.[2] Additionally, this technique minimizes solvent use and greatly reduces polymerization time, enabling facile production of commonly used materials, including adhesives,[3] foams,[4,5] and resins.[6,7] FP has been established for radical,[8,9] cationic,[10,11] and ring-opening metathesis polymerization (ROMP)[6,12] mechanisms to produce thermoplastics and thermosets from polyacrylates, epoxies, and polyolefins. Of the three FP methods, frontal ROMP (FROMP) is especially of interest because it produces ubiquitous polyolefins[6,13] and premature bulk polymerization can be easily prevented using well-known catalyst inhibition mechanisms.[14,15]
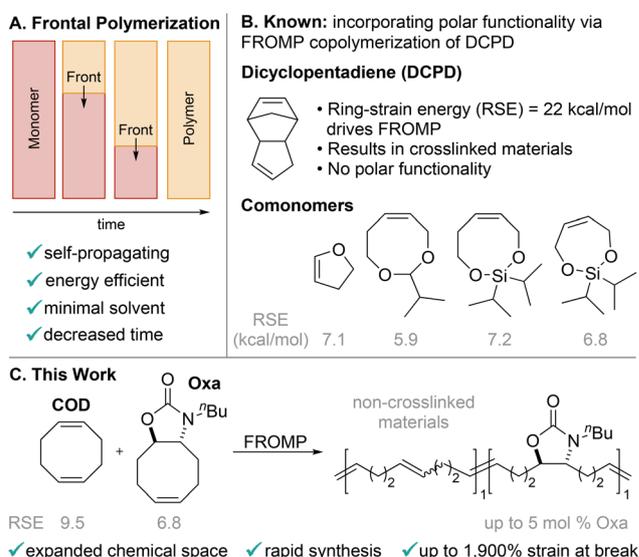

Fig. 1 (A) General scheme of front propagation and benefits of FP. (B) Previously reported comonomers for polar-functionalized p(DCPD) *via* FROMP. (C) FROMP copolymerization of COD with an oxazolidinone-fused cyclooctene (Oxa).

Department of Chemistry, University of Minnesota-Twin Cities, 207 Pleasant Street SE, Minneapolis, MN 55455, USA. E-mail: jrlamb@umn.edu

† These authors contributed equally to this work.

The FROMP exotherm is driven by the release of ring strain energy (RSE) of highly strained monomers. The most common monomer is dicyclopentadiene (DCPD, RSE = 22 kcal mol^{-1})[6,12,16,17] to produce crosslinked thermosets followed by cyclooctadiene (COD, RSE = 9.5 kcal mol^{-1})[18,19] to produce linear poly(1,4-butadiene).[13,20,21] Polar comonomers with lower RSE (5.9–7.2 kcal mol^{-1})[22,23] – such as enol ethers,[24] acetals,[23] and silyl ethers[23,25] (Fig. 1B) – have been copolymerized with DCPD to access broader materials and enable degradation. While copolymers of COD and DCPD have been studied,[13,26] COD has yet to be copolymerized with any polar comonomers *via* FROMP. Previously, we developed a ROMP-based synthesis of polyoxazolidinone (POxa) homopolymers,[27] a subclass of polyurethanes that contain strong (~5 Debye),[28] oriented dipoles in their repeat units. The orientation and strength of POxa dipoles have previously been shown to affect thermal and viscoelastic properties.[29] Therefore, we were interested in the effect of such strong dipoles on pCOD-based thermoplastics which we hypothesized could be rapidly synthesized *via* FROMP.

Herein, we utilize FROMP to copolymerize COD with an oxazolidinone-fused cyclooctene monomer (Oxa) to produce polar-functionalized polybutadienes on gram scale within minutes (Fig. 1C). Copolymers were synthesized with 1–5 mol% Oxa, depicted as p(COD-*co*-Oxa$_{x\%}$). Higher loadings resulted in slower front velocities and lower maximum front temperatures, reflecting the lower RSE of Oxa (6.8 kcal mol^{-1}, see SI, Sections S1A and S5).[27,30] While the degradation and glass transition (T_g) temperatures varied only slightly with increasing Oxa incorporation, the crystallinity was appreciably affected. We noted a sharp decrease of ~20 °C for the crystallization temperatures (T_c) and broader melting endotherms for all copolymers *versus* pCOD, suggesting inhibited crystallization and less-defined crystalline regions for Oxa-containing polymers. Furthermore, samples of p(COD-*co*-Oxa$_{5\%}$) reached ~1900% strain at break, a >8-fold increase over that of pCOD homopolymer. We hypothesize that this increased ductility arises from the lower T_c and introduction of transient, physical crosslinks from the Oxa dipoles. This work provides the first polar-functionalized pCOD synthesized *via* FROMP and establishes oxazolidinones as a valuable dipolar moiety for tuning thermal and mechanical properties of copolymers, even at low incorporation.

Results and discussion

Polymer synthesis

Oxa was a suitable comonomer for FROMP because its RSE is in line with previously reported FROMP comonomers[22,23] and it is a liquid at room temperature, which facilitates a homogenous solution with minimal solvent. We copolymerized COD with varying Oxa loadings in ~4 mm diameter glass tubes using 100 ppm of second-generation Grubbs catalyst (G2, see Fig. S6) relative to total monomer and 30 ppm of tributyl phosphite (TBP, see Fig. S6) inhibitor to prevent premature bulk polymerization. This inhibitor loading is lower than standard DCPD FROMP conditions (100 ppm)[23,31,32] to increase front velocity due to the lower RSE of our chosen monomers.[15] Copolymerizations and structural characterization were conducted in triplicate to quantify reproducibility. We observed full propagation of the polymerization front for p(COD-*co*-Oxa$_{1-5\%}$) (Table 1, entries 2–4), but increased Oxa loadings of 10 and 12 mol% yielded incomplete propagation (see Table S1). As a control, we attempted Oxa homopolymerization and observed no front formation, even in the absence of inhibitor (see SI, Section S2B). This result is unsurprising since FROMP homopolymerization has never been demonstrated on a monomer with lower RSE than COD.

Next, we measured front velocity and maximum front temperature (Table 1), which are used to probe the effect of kinetics, thermodynamics, and heat transfer on FP.[7] The front velocity was calculated from videos (see Video S1) analysed by Tracker 6.3.1® software[33] starting from visible front formation until the tube began to narrow (see SI, Section S3A). The front temperature was measured using a thermocouple positioned 15 mm deep in the monomer solution. First, we obtained front velocity for the homopolymerization of COD (0.535 mm s^{-1}, Table 1, entry 1) to compare with the previously reported[13] value (0.6 mm s^{-1} at 45 ppm of TBP). We attribute the slight discrepancy to the different surface area to volume ratios of the reaction vessels (see SI, Section S3A). As Oxa loadings increased, the front velocities were notably slowed, varying from 0.464 mm s^{-1} at 1 mol% to 0.269 mm s^{-1} at 5 mol% (Table 1, entries 2–4). These results were expected because lower RSE monomers have less of a thermodynamic driving force for polymerization, which is known to slow the kinetics of FROMP.[13,23,24] Similarly, the front temperature decreased by

Table 1 pCOD and p(COD-*co*-Oxa$_{1-5\%}$) polymers prepared through FROMP[a]

Entry	Mol% Oxa loading	Mol% Oxa incorporation[b,c]	M_n (kDa)[c,d]	$Đ$[c,d]	Front velocity (mm s^{-1})[e]	Front temperature (°C)[e]
1	0	0	117	2.3	0.535 ± 0.011	126.7 ± 0.8
2	1.0	1.1	150	2.2	0.464 ± 0.021	122.5 ± 3.1
3	3.0	3.2	177	2.2	0.383 ± 0.007	115.1 ± 2.6
4	5.0	5.2	133	2.0	0.269 ± 0.004	111.0 ± 2.2

[a] Standard conditions: [COD] + [Oxa] = 189 M in toluene, 100 ppm G2 and 30 ppm TBP relative to [total monomer]. [b] Obtained *via* ^{1}H NMR spectroscopy of polymer after quenching with ethyl vinyl ether, precipitating, and drying under vacuum at 60 °C overnight. [c] Values reported are averages of three replicates. [d] Obtained *via* SEC of precipitated polymer using a refractive index (RI) detector in THF against polystyrene standards. [e] Values reported are averages and one standard deviation of three replicates.

~16 °C between pCOD and p(COD-*co*-Oxa$_{5\%}$). Both of these results support incorporation of the polar comonomer. In contrast, our attempt to copolymerize Oxa with the higher RSE DCPD resulted in poor Oxa incorporation despite forming a propagating front (see SI, Section S2D).

The structures of the resulting p(COD-*co*-Oxa$_{1-5\%}$) were characterized by ^{1}H NMR and IR spectroscopies as well as size exclusion chromatography (SEC) to support the successful incorporation of Oxa. The ^{1}H NMR spectra of the precipitated copolymers showed all the expected peaks and actual incorporation of the Oxa repeat unit matched closely with the monomer feed ratio (Fig. 2A, Table S3). In the IR spectra, we observed the presence of the characteristic peak at ~1760 cm^{-1} corresponding to the C=O stretch of the oxazolidinone moieties (Fig. 2B, SI Section 3B). In SEC, all samples had monomodal distributions (Fig. S13) and number-average molar mass (M_n) values between 117 to 219 kDa (Table 1, Table S5). Dispersities (Đ) of ~2 were observed for all samples, which is in line with previously reported Đ values of pCOD synthesized *via* FROMP.[13]

Thermal characterization

With a series of four polyolefins in hand, we transitioned to investigating material properties, starting with thermal characterization. To prevent radical-mediated crosslinking over time, we treated samples with 0.5 wt% butylated hydroxytoluene (BHT).[27,29,34] BHT-treated pCOD was characterized in parallel

as a benchmark, and its properties were compared to previous reports[35–38] to ensure that the radical scavenger was not significantly affecting the properties.

First, we investigated thermal degradation of the polymers using thermogravimetric analysis (TGA). Oxa incorporation did not show significant changes to the degradation profile between polymers. All samples, including pCOD, show a 2-stage degradation, which is typical for polybutadiene.[35–37] Thus, we report two extrapolated onset degradation temperatures (T_o) for all samples: the first occurs at 357–360 °C and the second at 420–440 °C (see T_o calculation in SI, Section S1A).

Next, differential scanning calorimetry (DSC) was used to evaluate the thermal transitions of pCOD and p(COD-*co*-Oxa$_{1-5\%}$). PCOD displayed a T_g at −84 °C and multiple overlapping endothermic melting peaks, which are in agreement with previous reports.[13] Upon incorporation of Oxa, the T_g values do not change significantly, remaining within the range of −89 to −78 °C (Fig. 3A). Similarly, the T_m values only decrease by 15–16 °C, but pCOD's sharp peak at T_m = 33 °C disappears for p(COD-*co*-Oxa$_{1-5\%}$). The broadening of this endotherm indicates the well-defined crystallites in the homopolymer are less uniform in the copolymer. Since the POxa homopolymer is not semicrystalline[27] and Oxa is incorporated in relatively small amounts, we hypothesize that the crystalline regions are primarily pCOD with the Oxa repeat units clustering together outside of the lattice. These Oxa clusters likely depress the melting point *via* reduction in lamellae thickness of the pCOD regions.[39]

The T_c is also significantly influenced by the presence of Oxa repeat units. On the cooling cycle, pCOD displays a T_c at 22 °C, but all copolymers show a sharp exothermic peak
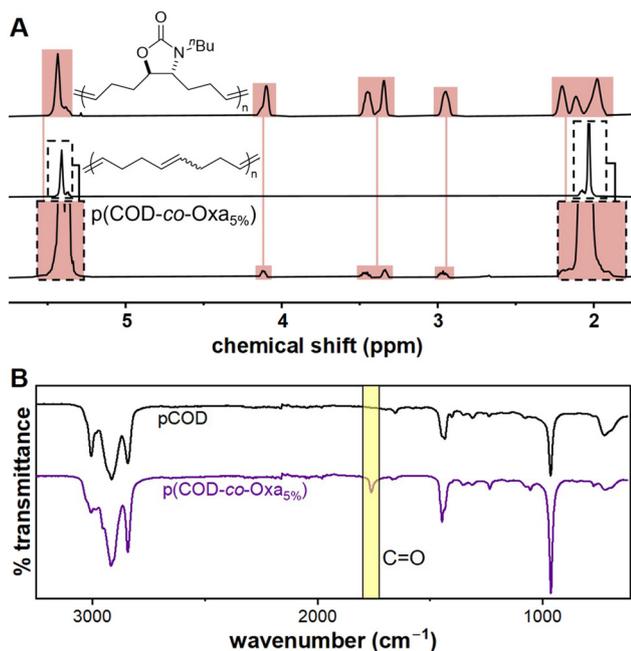

Fig. 2 (A) Stacked ^{1}H NMR spectra of POxa and pCOD homopolymers and p(COD-*co*-Oxa$_{5\%}$). The POxa homopolymer was synthesized through traditional ROMP using the following conditions: [Oxa] = 1.0 M in DCM, 4 mol% G2 at r.t. for 1 h. (B) Stacked ATR-IR spectra of pCOD, p(COD-*co*-Oxa$_{1\%}$) and p(COD-*co*-Oxa$_{5\%}$). The oxazolidinone C=O bond stretch region is highlighted in yellow.
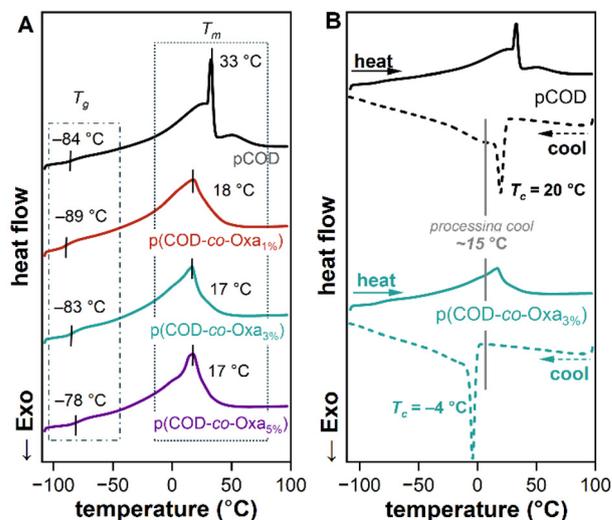

Fig. 3 (A) Stacked DSC thermograms showing T_g and T_m of pCOD and p(COD-*co*-Oxa$_{1-5\%}$) (B) DSC thermograms of the first cool (dashed) and the second heat (solid) of pCOD (top, black) and p(COD-*co*-Oxa$_{3\%}$) (bottom, teal). 15 °C (grey vertical line) indicates the approximate cooling temperature during processing prior to mechanical testing.

around 0 °C (Fig. 3B and S23–25). The lower T_c suggest that adding only a small amount of the Oxa moiety is disrupting the crystal lattice. We hypothesize that physical crosslinks arising from dipole–dipole interactions between the oxazolidinone clusters hinder crystallization.[40] This change in T_c has implications for polymer properties on the basis of the processing conditions (*vide infra*).

Mechanical characterization

In addition to Oxa incorporation affecting crystallinity, the stress–strain curves of pCOD and p(COD-*co*-Oxa$_{1-5\%}$) displayed stark differences in tensile properties (Fig. 4). Young's modulus (E) decreased monotonically with higher incorporation of the Oxa repeat unit from 5.72 to 1.09 MPa (Fig. 4 inset). Similarly, all polymers exhibited a yield point around 20% strain, with maximum stress decreasing as Oxa loading increased (see SI Section S3E). These trends imply that the addition of Oxa results in materials that are softer and easier to deform compared to pCOD homopolymer. While the low E and maximum stress are not advantageous for many thermoplastic applications, the subsequent increase in ductility (*i.e.*, strain at break) makes these materials an interesting system to study for potential thermoset applications in the future. The pCOD homopolymer samples failed at 220% strain, while Oxa loadings of 3 and 5 mol% increased the strain at break to 1540% and 1900%, respectively (see Table S6 for full tabulation and standard deviations). Notably, these samples reached

these incredible elongations while being pulled at a relatively fast extension rate (50 mm s^{-1}). The toughness of the material, represented by the area under the stress–strain curve, starkly decreased between pCOD and p(COD-*co*-Oxa$_{1\%}$) (3.05 to 0.663 MJ m^{-3}, respectively) due to the decrease in stress and little gain in elongation (Fig. 4). As Oxa loading increased to 3 and 5 mol% and elongation increased in turn, the materials recovered their toughness up to 2.30 MJ m^{-3}.

The dramatic differences between pCOD and the copolymers can be partially explained by the processing parameters. A uniform processing protocol was used for consistency rather than customizing to match the thermal events of each polymer. Tensile samples were melt pressed at 120 °C for 5 min, rapidly cooled to ~15 °C for 3 min, then stored at room temperature for 18–24 h (see SI, Section S3D for full procedure). For pCOD, this processing cool is *below* the T_c, while for Oxa-containing copolymers, this processing cool is *above* the T_c (Fig. 3B). The difference means that pCOD could recrystallize after melting, while the copolymers remained amorphous. This lack of crystallinity cannot be the only factor influencing the rubbery behaviour of the polymers, however, because the ductility continued to increase with higher Oxa loadings despite all copolymers having very similar T_c values (Fig. S30). We hypothesize that the rigid, strongly polar Oxa groups clustered outside of the pCOD lamellae (*vide supra*, thermal characterization) can create transient physical crosslinks, which break and reform during elongation to make the polymer more rubbery. Physical crosslinks arising from hydrogen bonding,[41,42] ionic dipoles,[43,44] and metal mediation[45,46] have been shown to influence properties such as toughness, mechanical strength, and viscoelasticity.

Fig. 4 Representative stress–strain curves of pCOD and p(COD-*co*-Oxa$_{1-5\%}$). Inset of stress–strain curves up to 60% strain is shown to highlight the difference in Young's Modulus (E) between pCOD and p(COD-*co*-Oxa$_{5\%}$). For a graph depicting curves up to 100% strain for all samples, please see SI, Fig. S31. Graphical depiction on the right-side shows hypothesized transient physical crosslinks arising from Oxa dipoles.

Conclusions

In summary, we copolymerized COD and Oxa at varying mole ratios to produce polar-functionalized polybutadienes *via* FROMP. This is the first example of a frontally polymerized material with oxazolidinone units, as well as the first report conducting FROMP between COD and a polar comonomer. The resulting linear materials are complementary to the known polar-functionalized crosslinked thermosets produced from DCPD copolymerization. We successfully synthesized p(COD-*co*-Oxa) copolymers with up to 5 mol% Oxa. We observed complete front propagation as well as an expected decrease in front velocity and temperature with increased Oxa loading on the basis of its lower RSE. While thermal degradation profiles and T_g remained similar across all samples, crystallinity was inhibited upon introduction of the polar comonomer. Additionally, polymers with more Oxa demonstrated impressively high strain at break compared to pCOD, indicating the transformation into highly ductile materials. Future work will explore further development of Oxa-based copolymers and potential applications of these emergent materials.
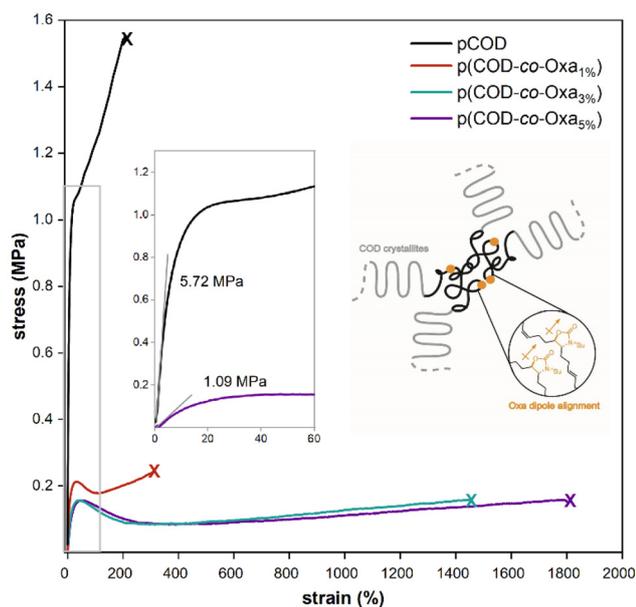
Author contributions

The manuscript was written through contributions of all authors. All authors have given approval to the final version of the manuscript. Credit: **Jazmin E. Aguilar-Romero** conceptualization, data curation, formal analysis, investigation, methodology, validation, visualization, writing – original draft, and writing – review & editing; **Elizabeth G. Rogan** data curation, formal analysis, investigation, methodology, visualization, writing – original draft, and writing – review & editing; **Allison R. Wong** data curation, formal analysis, investigation, and writing – review & editing; **Brandon M. Hosford** data curation, formal analysis, investigation, and writing – review & editing; **Angela L. Mosconi** investigation; **Jessica R. Lamb** conceptualization, formal analysis, funding acquisition, project administration, resources, supervision, writing – original draft, and writing – review & editing.

Conflicts of interest

There are no conflicts to declare.

Note added after first publication

Details in ref. 19 and 30 have now been corrected. The RSC apologies for this error in production. Furthermore, some minor formatting changes have been made to the style in which units have been displayed throughout the manuscript.

Data availability

The primary data files are archived with the Data Repository for the University of Minnesota and accessible *via* **https://doi.org/10.13020/7fxw-6g59**. Accompanying this manuscript is an SI file detailing experimental procedures, materials, and sample characterizations. See DOI: **https://doi.org/10.1039/d5py00721f**.

Acknowledgements

References

1 J. A. Pojman, in *Polymer Science: A Comprehensive Reference*, ed. K. Matyjaszewski and M. Möller, Elsevier, Amsterdam, 2012, pp. 957–980.

2 I. D. Robertson, M. Yourdkhani, P. J. Centellas, J. E. Aw, D. G. Ivanoff, E. Goli, E. M. Lloyd, L. M. Dean, N. R. Sottos, P. H. Geubelle, J. S. Moore and S. R. White, *Nature*, 2018, **557**, 223–227.

3 T. Holt, K. Fazende, E. Jee, Q. Wu and J. A. Pojman, *J. Appl. Polym. Sci.*, 2016, **133**, 44064.

4 D. M. Alzate-Sanchez, M. M. Cencer, M. Rogalski, M. E. Kersh, N. Sottos and J. S. Moore, *Adv. Mater.*, 2022, **34**, 2105821.

5 J. Park and S.-Y. Kwak, *Commun. Chem.*, 2022, **5**, 119.

6 A. Mariani, S. Fiori, Y. Chekanov and J. A. Pojman, *Macromolecules*, 2001, **34**, 6539–6541.

7 B. A. Suslick, J. Hemmer, B. R. Groce, K. J. Stawiasz, P. H. Geubelle, G. Malucelli, A. Mariani, J. S. Moore, J. A. Pojman and N. R. Sottos, *Chem. Rev.*, 2023, **123**, 3237–3298.

8 I. D. Robertson, H. L. Hernandez, S. R. White and J. S. Moore, *ACS Appl. Mater. Interfaces*, 2014, **6**, 18469–18474.

9 J. A. Pojman, V. M. Ilyashenko and A. M. Khan, *J. Chem. Soc., Faraday Trans.*, 1996, **92**, 2825–2837.

10 H. Švajdlenková, A. Kleinová, O. Šauša, J. Rusnák, T. A. Dung, T. Koch and P. Knaack, *RSC Adv.*, 2020, **10**, 41098–41109.

11 B. R. Groce, D. P. Gary, J. K. Cantrell and J. A. Pojman, *J. Polym. Sci.*, 2021, **59**, 1678–1685.

12 I. D. Robertson, E. L. Pruitt and J. S. Moore, *ACS Macro Lett.*, 2016, **5**, 593–596.

13 L. M. Dean, Q. Wu, O. Alshangiti, J. S. Moore and N. R. Sottos, *ACS Macro Lett.*, 2020, **9**, 819–824.

14 T. E. Schmid, X. Bantreil, C. A. Citadelle, A. M. Z. Slawin and C. S. J. Cazin, *Chem. Commun.*, 2011, **47**, 7060–7062.

15 I. D. Robertson, L. M. Dean, G. E. Rudebusch, N. R. Sottos, S. R. White and J. S. Moore, *ACS Macro Lett.*, 2017, **6**, 609–612.

16 A. Ruiu, D. Sanna, V. Alzari, D. Nuvoli and A. Mariani, *J. Polym. Sci., Part A: Polym. Chem.*, 2014, **52**, 2776–2780.

17 P. R. Khoury, J. D. Goddard and W. Tam, *Tetrahedron*, 2004, **60**, 8103–8112.

18 N. L. Allinger and J. T. Sprague, *J. Am. Chem. Soc.*, 1972, **94**, 5734–5747.

19 The RSE for COD was previously reported as 13 kcal mol^{-1} in 1972 (ref. 18). We repeated this calculation using the same DFT method used for the Oxa RSE calculation so we could better compare these monomers. This more modern method calculated the RSE of COD to be 9.5 kcal mol^{-1} (see SI, Section 5).

20 Y. Gao, M. A. Dearborn, S. Vyas, A. Kumar, J. Hemmer, Z. Wang, Q. Wu, O. Alshangiti, J. S. Moore, A. P. Esser-Kahn and P. H. Geubelle, *J. Phys. Chem. B*, 2021, **125**, 7537–7545.

21 J. E. Paul, Y. Gao, Y. K. Go, L. E. Rodriguez Koett, A. Sharma, M. Chen, J. J. Lessard, T. Topkaya, C. Leal, J. S. Moore, P. H. Geubelle and N. R. Sottos, *Nature*, 2024, **634**, 85–90.

22 T.-G. Hsu, S. Liu, X. Guan, S. Yoon, J. Zhou, W.-Y. Chen, S. Gaire, J. Seylar, H. Chen, Z. Wang, J. Rivera, L. Wu, C. J. Ziegler, R. McKenzie and J. Wang, *Nat. Commun.*, 2023, **14**, 225.

23 E. M. Lloyd, J. C. Cooper, P. Shieh, D. G. Ivanoff, N. A. Parikh, E. B. Mejia, K. E. L. Husted, L. C. Costa, N. R. Sottos, J. A. Johnson and J. S. Moore, *ACS Appl. Eng. Mater.*, 2023, **1**, 477–485.

24 O. Davydovich, J. E. Paul, J. D. Feist, J. E. Aw, F. J. Balta Bonner, J. J. Lessard, S. Tawfick, Y. Xia, N. R. Sottos and J. S. Moore, *Chem. Mater.*, 2022, **34**, 8790–8797.

25 P. Shieh, W. Zhang, K. E. L. Husted, S. L. Kristufek, B. Xiong, D. J. Lundberg, J. Lem, D. Veysset, Y. Sun, K. A. Nelson, D. L. Plata and J. A. Johnson, *Nature*, 2020, **583**, 542–547.

26 J. C. Cooper, J. E. Paul, N. Ramlawi, C. Saengow, A. Sharma, B. A. Suslick, R. H. Ewoldt, N. R. Sottos and J. S. Moore, *Adv. Mater.*, 2024, **36**, 2402627.

27 A. Pal, A. R. Wong and J. R. Lamb, *ACS Macro Lett.*, 2024, **13**, 502–507.

28 C. M. Lee and W. D. Kumler, *J. Am. Chem. Soc.*, 1961, **83**, 4596–4600.

29 A. R. Wong, J. Barroso, L. G. Wetherbee, B. Vlaisavljevich and J. R. Lamb, *J. Am. Chem. Soc.*, 2025, **147**, 28350–28358.

30 The RSE for Oxa was previously reported as 7.4 kcal mol^{-1} in 2024 (ref. 27). This more modern DFT method calculated the RSE of Oxa to be 6.8 kcal mol^{-1} (see SI, Section 5).

31 H. Liu, H. Wei and J. S. Moore, *ACS Macro Lett.*, 2019, **8**, 846–851.

32 D. G. Ivanoff, J. Sung, S. M. Butikofer, J. S. Moore and N. R. Sottos, *Macromolecules*, 2020, **53**, 8360–8366.

33 D. Brown, C. Wolfgang and R. M. Hanson, *Tracker (version 6.3.1)*.

34 W. A. Yehye, N. A. Rahman, A. Ariffin, S. B. Abd Hamid, A. A. Alhadi, F. A. Kadir and M. Yaeghoobi, *Eur. J. Med. Chem.*, 2015, **101**, 295–312.

35 D. W. Brazier and N. V. Schwartz, *J. Appl. Polym. Sci.*, 1978, **22**, 113–124.

36 F. Li, Y. Gao, C. Yu, H. Yang, G. G. Liu, W. Cao and J. Guo, *J. Appl. Polym. Sci.*, 2024, **141**, e55556.

37 J.-P. Lin, C.-Y. Chang, C.-H. Wu and S.-M. Shih, *Polym. Degrad. Stab.*, 1996, **53**, 295–300.

38 L. M. Pitet and M. A. Hillmyer, *Macromolecules*, 2009, **42**, 3674–3680.

39 T. P. Lodge and P. C. Hiemenz, *Polymer Chemistry*, CRC Press, Taylor and Francis Group, Boca Raton, FL, 3rd edn, 2020.

40 E. Kontou, G. Spathis, M. Niaounakis and V. Kefalas, *Colloid Polym. Sci.*, 1990, **268**, 636–644.

41 Y. Zhuo, Z. Xia, T. Qi, T. Sumigawa, J. Wu, P. Šesták, Y. Lu, V. Håkonsen, T. Li, F. Wang, W. Chen, S. Xiao, R. Long, T. Kitamura, L. Li, J. He and Z. Zhang, *Adv. Mater.*, 2021, **33**, 2008523.

42 J. A. Neal, D. Mozhdehi and Z. Guan, *J. Am. Chem. Soc.*, 2015, **137**, 4846–4850.

43 J. A. Jaber and J. B. Schlenoff, *J. Am. Chem. Soc.*, 2006, **128**, 2940–2947.

44 B. Han, D. R. Chery, J. Yin, X. L. Lu, D. Lee and L. Han, *Soft Matter*, 2016, **12**, 1158–1169.

45 H. Park, T. Kang, H. Kim, J.-C. Kim, Z. Bao and J. Kang, *Nat. Commun.*, 2023, **14**, 5026.

46 Y. Chen, P. G. Miller, X. Ding, C. E. T. Stowell, K. M. Kelly and Y. Wang, *Adv. Mater.*, 2020, **32**, 2003761.